Damage in dual phase steel DP1000 investigated using digital image correlation and microstructure simulation

2015 Modelling Simul. Mater. Sci. Eng. 23 085005

(http://iopscience.iop.org/0965-0393/23/8/085005)

OPEN ACCESS
IOP Publishing
Modelling and Simulation in Materials Science and Engineering
Modelling Simul. Mater. Sci. Eng. **23** (2015) 085005 (17pp) doi:10.1088/0965-0393/23/8/085005

Damage in dual phase steel DP1000 investigated using digital image correlation and microstructure simulation

Khaled Alharbi[1], Hassan Ghadbeigi[1], Panos Efthymiadis[2], Mohammad Zanganeh[1], Steven Celotto[3], Richard Dashwood[2] and Christophe Pinna[1]

[1] The University of Sheffield, Department of Mechanical Engineering, Mappin street, Sheffield S1 3JD, UK
[2] WMG, University of Warwick, Coventry CV4 7AL, UK
[3] Tata Steel R&D, IJmuiden, The Netherlands

E-mail: kfmalharbi1@sheffield.ac.uk

Received 17 November 2014, revised 30 June 2015
Accepted for publication 14 August 2015
Published 9 October 2015

Abstract

Microstructure failure mechanisms and void nucleation in dual-phase (DP) steels during deformation have been studied using a combination of *in situ* tensile testing in a scanning electron microscope (SEM), digital image correlation (DIC) and finite element (FE) modelling. SEM images acquired during *in situ* tests were used to follow the evolution of damage within the microstructure of a DP1000 steel. From these images, strain maps were generated using DIC and used as boundary conditions for a FE model to investigate the stress state of martensite and ferrite before the onset of the martensite phase cracking. Based on the simulation results, a maximum principal stress of about 1700 MPa has been estimated for crack initiation in the martensite of the investigated DP1000 steel. The SEM image observations in combination with the FE analyses provide new insights for the development of physically-based damage models for DP-steels.

Keywords: dual-phase steels, digital image correlation, microstructure simulation, martensite fracturing

(Some figures may appear in colour only in the online journal)

1. Introduction

Advanced high strength steels (AHSS) have the advantage of combined high strength and high ductility. This combination of mechanical properties makes them useful in automotive applications where high strength is desirable for weight reduction through down-gauging and for crash resistance, while the large fracture strain is important for good formability. Dual-phase (DP) steels are the most common type of AHSS and have relatively large uniform elongation that makes them most suitable for deep drawing and other stretch-forming based manufacturing processes.

The microstructure of DP-steels consists of hard martensite islands in a soft ferrite matrix. This combination of hard and soft microstructure constituents leads to strain partitioning at the microscopic level, which produces the useful mechanical properties mentioned earlier. The strength and ductility of DP-steels not only depend on the volume fraction of the martensite, but also on the morphology and intrinsic mechanical properties of this secondary microstructure constituent [1–3]. The enhancement of DP-steels' properties for current and future applications requires a critical investigation of the deformation and damage mechanisms operating at the micro-scale in order to understand and predict their behaviour.

In order to understand the damage evolution in DP-steels, local strain distribution within the microstructure has been studied by several researchers using digital image correlation (DIC). Kang *et al* [4] studied damage initiation using DIC in DP600 with varying microstructures. A comparison was made between inter-critically annealed (i.e. in the temperature regime where both ferrite and austenite are stable) and quenched (to transform the austenite into martensite) sheets to material that was subsequently tempered at 450 °C for 1 h and then slow cooled. Tempering reduced the hardness differential by softening the martensite and hardening the ferrite. The tempered material deformed more before damage was observed compared to the as-quenched only samples. The local strain for the initiation of damage (i.e. voids between two martensite islands) increased from 40% in the annealed-quenched sample to 60% in the tempered sample. The damage then progressed by either fracturing through the ferrite grains or along the interface between ferrite and martensite. Ososkov *et al* [5] also used DIC to examine the strain partitioning in DP600 steels and they reported local strain values within martensite-rich areas with a maximum value of 30% and a maximum strain of 70% in the ferrite. Ghadbeigi *et al* [6] utilised *in situ* tensile tests inside a SEM and used DIC to measure the strain fields in DP1000 during the deformation. The tests were interrupted at regular intervals in order to capture SEM images of the deformed microstructure. These images were analysed using DIC to measure the local plastic strain evolution in martensite and ferrite. Two damage mechanisms were observed, the most common being the de-cohesion of the interface between martensite and ferrite followed by martensite fracture. Voids in the ferrite phase nucleated in regions with a local strain of 120%.

So far, damage has been characterised in relation to strain distributions because DIC can only measure displacements and, by differentiation, strain values. Stress distributions can be obtained with the aid of finite element (FE) modelling and such microstructure-based simulation has been a topic of active research over the past decade. Some investigators use microstructure modelling based on the realistic representations of the constituent morphology and distributions to study the deformation and damage mechanisms of DP-steels. Kadkhodapour *et al* [7] proposed two void initiation models based upon experimental observations and simulation results of commercial DP800 steels. Elongated voids were more likely to form as a result of decohesion of ferrite-ferrite interfaces in regions with long grain boundaries surrounded by martensite particles. It was shown that strain incompatibility led to stress concentration in these areas. The second mechanism observed was the formation of spherical voids in small ferrite grains constrained between martensite particles. The high hydrostatic pressure found in this region initiated void nucleation by the mechanism that was claimed to be decohesion of the

interface between ferrite and martensite. Sun *et al* [8] used microstructure modelling to study the key factors influencing the failure mechanisms of DP-steels with different volume fractions. In DP-steels with less than 15% of martensite, the growth and coalescence of pre-existing microvoids in the ferrite phase was shown to be the dominant cause of damage. However, at higher volume fractions up to 40%, the incompatibility between hard martensite and soft ferrite significantly influenced damage, whereas the pre-existing microvoids were no longer the main factor.

This paper examines the damage development in commercial DP1000 steels using both local strain and stress analysis. The deformation of the microstructure was first measured experimentally using DIC and the measured displacement values were then used as boundary conditions for a microstructural FE model. *In situ* tensile tests were performed inside a SEM chamber to observe the actual deformation of DP1000 microstructure and the subsequent micrographs were analysed using DIC. 2D models were then generated from SEM images of the imaged microstructure of DP1000 and stress values at damage locations were analysed.

2. Experimental procedure

The material used in this study is a commercial cold rolled uncoated DP1000 steel grade consisting of 60% martensite (light regions) embedded in ferrite (dark regions) with approximate average grain size of 7 μm as shown in figure 1(a). The microstructure in figure 1(a) shows a contiguous martensite network that is relatively homogenous and has no banding in the rolling direction. The material was provided in the form of 1.5 mm thick sheets. The chemical composition is given in table 1.

The main aim of the experiment was to progressively follow the deformation of the microstructure at the surface of a DP1000 sample during tensile testing. A Deben Microtest tensile stage with 5 kN maximum load capacity was used. Special dog bone specimens, shown in figure 1(b), were designed to ensure specimens failed below the maximum allowed load and extension of the tensile stage. A small 2×2 mm gauge section was chosen in order to make the observation of damage initiation easier by localising the deformation. Two sets of specimens were manufactured in the rolling and along the transverse direction. The tests were displacement controlled with a rate of 0.1 mm min^{-1} [6].

Before tensile testing, the DP1000 specimens were metallographically polished and then etched with 5% Nital for 5 s to reveal the microstructure as shown in figure 1(a). The experiments were run inside a CamScan MK II SEM chamber and interrupted at regular intervals during the tensile tests until fracture to record secondary-electron micrographs of the deformation history and damage development.

DIC was used for quantitative deformation analysis and local strain calculation using LaVision 7.1 software [9]. The technique discretises the undeformed image into small interrogation or subset windows, each having a unique pixel intensity array. A correlation algorithm is used to track the windows in the deformed images and calculate displacement vectors at the centre of each subset. Once these are known, in-plane strain values can be computed through differentiation. A detailed description and explanation of the DIC technique can be found in [10, 11]. The strain values were determined using the SEM images taken after each successive loading step in order to obtain the full history of the strain field from undeformed configuration up to fracture. Microstructural features have been used directly for the correlation, without any filtering or image corrections. A reduced pass algorithm [9] was used starting from 12.5×12.5 μm^2 (64×64 pixel^2) interrogation windows for the first pass and reduced to 6.25×6.25 μm^2 (32×32 pixel^2) for the second pass with 50% overlap. An example of initial and final interrogation windows and their respective overlap is shown in figure 1(a) with respect

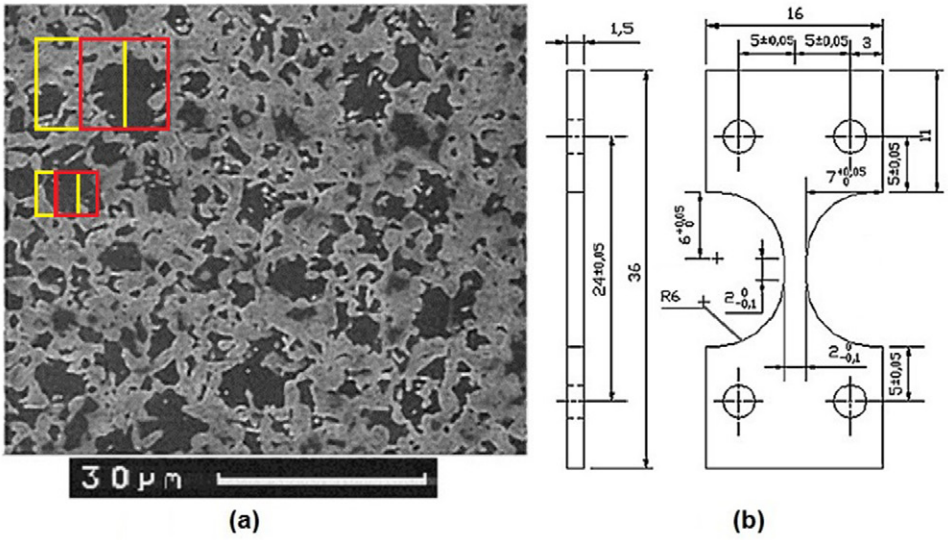

Figure 1. (a) SEM image of the DP1000 microstructure with overlaid squares representing the interrogation windows used for DIC analysis and (b) specimen dimensions in mm.

Table 1. Weight percentage (wt%) chemical composition of the DP1000 steel.

C	Mn	Si	Cr	V	Ni	Nb
0.152	1.53	0.474	0.028	0.011	0.033	0.014

to the microstructure. This procedure gives an accuracy of 0.005 μm for the displacement vectors and about 0.3% for strain values [9]. This DIC procedure for computing strain distributions over areas of microstructures has been validated against an independent technique in [12].

3. Microstructure modelling

Microstructure simulation is used to study the observed damage in terms of stress state. A MatLab [13] code developed by Chalon [14], creates an input file for Abaqus version 6.10 [15] using a 2D mesh of the microstructure based upon the SEM images taken in this work. The code divides the image into subset windows and converts each subset into a square element with four nodes. The linear quadrilateral element CPS4R was used in the simulations. The code then assigns each element to either ferrite or martensite according to the grey intensity level in the SEM image, after a threshold operation is used to convert the original image into a black and white picture. Figure 2(a) shows an image of the generated model for the area of interest in the SEM image of the undeformed DP1000 microstructure.

Another MatLab code was created to define the boundary conditions of the model in the Abaqus input file. The boundary conditions for the analysed area were imported from the DIC results with displacement values along the X and Y directions assigned to all nodes of the modelled area. As a result, the simulation is expected to represent the actual deformation of the analysed area. The model assumes a perfectly cohesive interface between the two microstructure constituents.

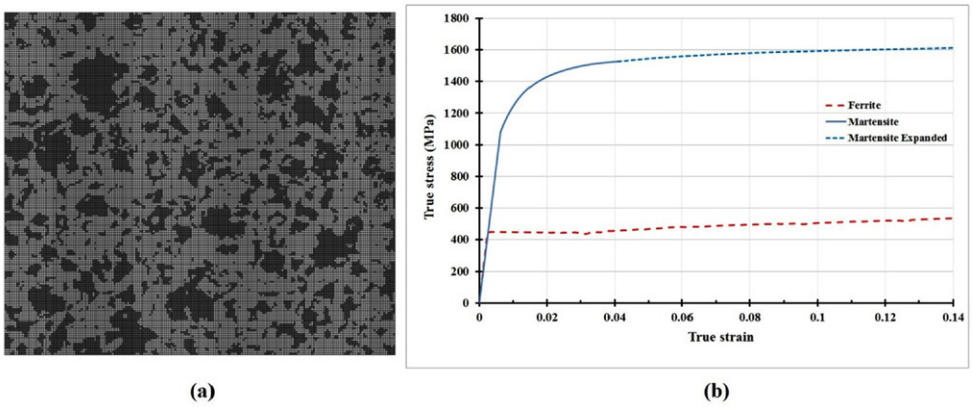

Figure 2. (a) Gray (ferrite) and white (martensite) microstructure model generated from the SEM image in figures 1(b) and (b) flow curves of martensite (blue) and ferrite phase (red) of DP1000.

Pure martensite and pure ferrite stress/strain curves were measured from strip fabricated to have the chemical composition and microstructure of the individual constituents, i.e. low-carbon ferrite and high-carbon martensite. The measured stress/strain curves of these two materials were then inputted into the FE model. The local stress/strain response of ferrite and martensite within the two-phase material is likely to differ from that measured on pure phase specimens. Consequently, finite element simulations of the deforming microstructure have been used to adjust these local flow curves by minimising the error between the averaged modelling stress and the experimental true stress value.

Five deformed images were simulated for stages after yielding through to the ultimate tensile strength point. The average stress of each state is calculated and compared to the applied experimental true stress of the whole specimen. Averaging the microstructure stress fields can be conducted using the following relation:

$$\overline{\sigma} = \frac{1}{V}\int_V \sigma \mathrm{d}V \tag{1}$$

$\overline{\sigma}$ is the average stress, V is the total volume of the microstructure model and σ is the stress computed at every Gauss point in the model [16–18]. The model used here is 2D with plane stress condition and unit thickness. The von Misses stress computed in every element was then averaged according to equation (1).

Table 2 summarises the comparison between modelling results and experimental values. A maximum error of 3.2% can be observed. This is relatively small and can be related to a discrepancy between the model and the actual material in terms of microstructure constituent properties or/and a 3D effect as the model was run under plane stress conditions.

Both the ferrite and martensite are considered here to have an elastic–plastic behaviour with an isotropic hardening law. The sensitivity to crystal orientation and sub-surface morphology on the calculated stresses were not included in the model and these assumptions may affect the results as will be discussed later.

Figure 2(b) shows the adjusted flow curves of martensite and ferrite defined in the model. The martensite strips fractured at an applied true strain of about 3.8%. However, results from the literature have shown that the martensite phase in DP-steels can plastically deform to a larger extent with measured local strain values larger than 10% [6]. Consequently, the stress/

Table 2. Comparison between experimental true stress and simulated average stress values during the uniform elongation of the specimen.

Applied strain (%)	**2**	**4**	**7**	**9**	**11**
True stress (MPa)	1012	1076	1135	1168	1196
Model average stress (MPa)	980	1045	1104	1132	1167
Error (%)	3.2	2.9	2.7	3.1	2.5

strain curve for martensite was artificially extrapolated with the same slope of the curve as that just before the measured data terminates. The elastic modulus values of 198 GPa and 182 GPa were used for ferrite and martensite respectively and a Poisson's ratio value of 0.3 for both phases. These values were calculated from the data acquired from tensile experiments on martensitic and ferritic strips.

4. Results

Figure 3 presents the measured engineering tensile stress strain curves for the DP1000 material tested in the rolling and transverse directions. There is little difference between the two directions, which shows that there is a low level of anisotropy in the material. This correlates well to the observation that the two phases are uniformly distributed in both directions without any particular banding, as can be seen in the micrograph shown in figure 2(a). From the data in figure 3, the yield strength is about 950 MPa and the ultimate tensile strength (UTS) is approximately 1110 MPa, which is indicative that the material is a high yield type of DP-steel. As a consequence of the small gauge length tensile specimen geometry used, the uniform strain was 14% and the fracture strain 48%, both of which are almost a factor of five greater than for a DP1000 steel tested using standard geometries. However, this gave the opportunity to observe the development of microstructure deformation and damage in such high strength steel grades that have relatively limited post-uniform elongation. The regular stress relaxations seen in the tensile curve here are due to the interruption of the test to acquire SEM images of the deformed microstructure for subsequent DIC analysis.

4.1. Damage observation

The SEM images have been analysed in order to investigate the initiation and development of damage in DP1000 steel specimens. Ductile failure usually involves void initiation, propagation and coalescence. Void initiation in DP-steels can be created by two types of microstructure constituents: (i) martensite islands or (ii) non-metallic inclusions (NMI). NMI's are undesirable particles formed in the material during the steel making and casting process. Figure 4 shows such an NMI at the centre of the field of view, surrounded by a characteristic cavity that typically forms during specimen preparation as a consequence of chemical dissolution by polishing and etching media. The interpretation that this feature is a NMI is based on this characteristic cavity, but also on how the particle behaved in brittle manner upon deformation and its similarity to other such particles that were found to contain aluminium and oxygen using energy dispersive spectroscopy in the SEM as shown in figure 5.

At the early stages of the uniform deformation, after an applied specimen strain of 2% as measured from the grip displacement, the NMI particle had already fractured and thus, was the first microstructural feature to exhibit damage. Since the NMI fractured, it shows that the surrounding cavity was only at the surface and the rest of the particle was indeed attached to the surrounding metal. However, upon further macroscopic deformation, apart from enlarging

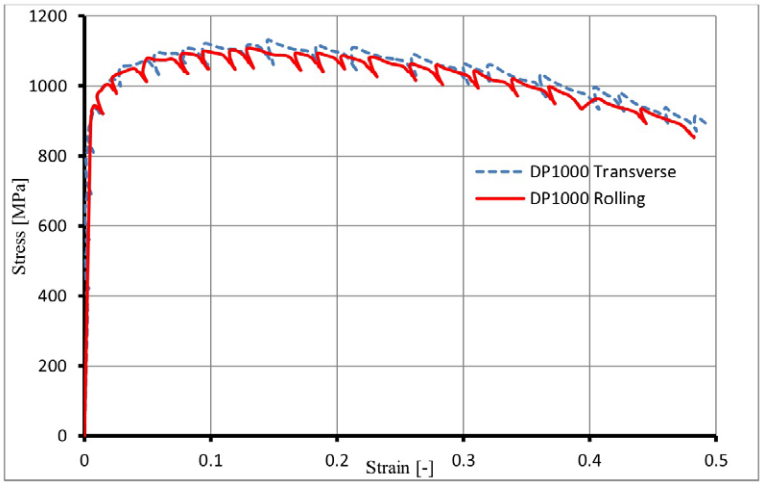

Figure 3. Stress–strain curves of DP1000 steels for specimens loaded parellel to the rolling direction (red) and perpenducular to the rolling direction (blue).

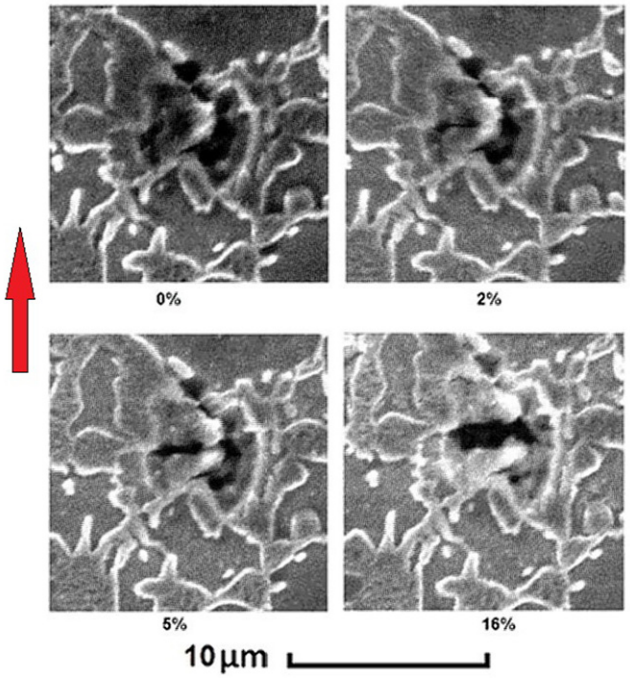

Figure 4. Void nucleation and growth with related applied strain due to an NMI in the material (the loading direction is shown with the red arrow on the left hand side).

of the surrounding surface cavity, no crack developed into the surrounding ferrite-martensite microstructure. This suggests that in this case at least, the NMI was relatively innocuous.

Martensite is the main microstructure constituent in DP-steel that imparts strength to the material. Figure 6 shows the progression in the void development near martensite islands as

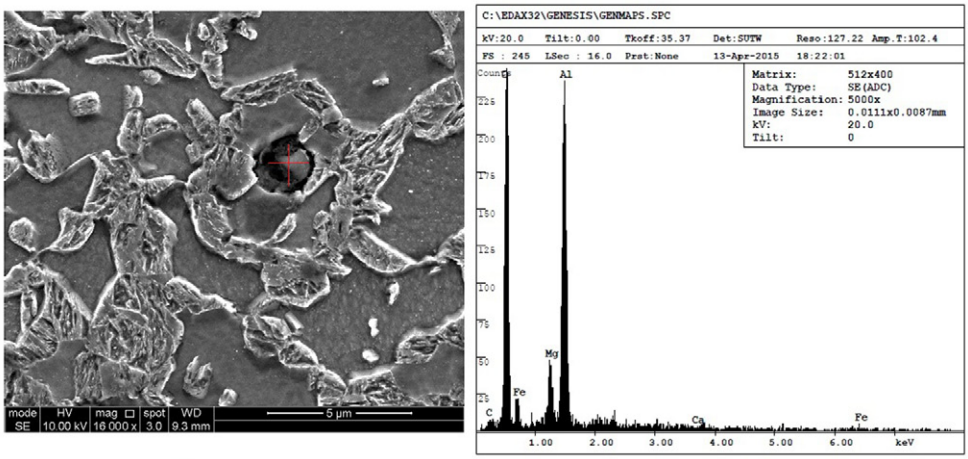

Figure 5. (a) SEM image of a NMI and (b) energy dispersive spectroscopy analysis.

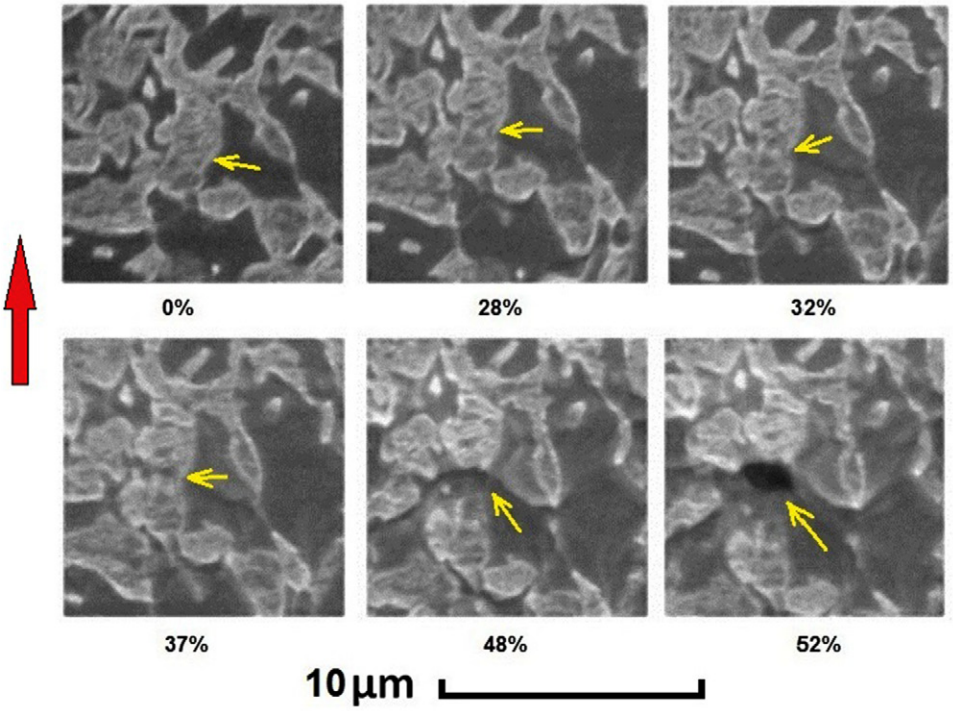

Figure 6. Spherical void nucleation as a result of martensite breaking and seperation in DP1000 steels, the applied specimen strain is indicated underneath each image (the loading direction is shown with the red arrow on the left hand side).

the applied specimen strain increased. Severe deformation occurred at a specimen strain value of 32%, shown by the local extension of the ferrite-martensite interface at the location where the martensite ultimately fractured. A crack then initiated at a small notch-like feature in the

martensite phase that was likely to have been a stress concentrator. The crack then propagated through the martensite phase. After the failure of the martensite phase, a spherical void formed as shown in figure 6 for when the applied specimen strain was 52%. At this stage the damage had propagated into the ferrite phase adjacent to where the now divided martensite island was.

Figure 7 shows an example of three different areas in the microstructure where damage developed as the applied specimen strain increased. These areas were chosen because damage appeared first in these clearly deformed regions. Damage initiated at the interface between ferrite and martensite at applied specimen strain of 16%, which is just after the UTS is reached. This damage then propagated through martensite islands until full separation at an applied specimen strain of about 37%. The mechanism observed in figure 7 is representative of the martensite failure observed at various positions in the microstructure of DP1000 during the test.

4.2. Strain distribution

This section describes the strain field analysed using DIC over the microstructure. Figure 8(a) shows the E_{yy} strain map (the y-axis corresponding to the tensile direction shown in the figure) for an applied specimen strain of 16%. At this strain level, no microstructural damage was observed and thus, it was chosen for further analysis because any voids or cracks would make the DIC measurement results unreliable around the defect area. As can be seen from figure 8(a), a maximum strain value of about 20% is observed in the large ferrite grain areas, whereas the minimum values are found in the predominantly martensite regions, as would be expected. In addition, strain bands orientated at 45^{o} (dashed lines) with respect to the loading direction (vertical in the figure) can be observed.

Figure 8(b) shows the distribution of strain values along the loading direction in both the martensite and ferrite for the area outlined by the box in figure 8(a). The distributions indicate that ferrite and martensite have deformed to similar degrees, with a slightly higher mean value for the softer ferrite (9.2% as opposed to 8.6% in the martensite). However, the difference is small and this might be owing to the high volume fraction of martensite in this material (about 60%). Standard deviation values of 2.4 for ferrite and 2.0 for martensite also show a similar strain heterogeneity for both phases.

4.3. Microstructure simulation

In order to investigate stress distribution in relation to the fracture process of martensite islands in DP1000 steel, the simulation results of the model shown in figure 2(a) were analysed. Figure 9(a) illustrates von-Mises stress results of ferrite and martensite in DP1000 for the microstructure shown in figure 1(a). The modelled area is highlighted with a black box in figure 8(a), for an applied specimen strain of 16%. Figure 9(b) shows the von Mises stress distribution in martensite and ferrite from the results in figure 9(a). Unlike strain, the von Mises stress distributions of martensite and ferrite are very different. As can be seen from figure 9(b), stress values in martensite are about three times higher than those in ferrite. The mean stress values are about 505 MPa and 1535 MPa for ferrite and martensite respectively. A larger standard deviation of 14 is observed for stresses in the ferrite matrix as compared to a standard deviation of 4 in martensite. This clearly shows that stress distribution is significantly more heterogeneous in the softer phase.

With respect to damage analysis, martensite fracturing was clearly observed in three areas of the region analysed with DIC (shown in figure 7) and consequently, these areas were chosen

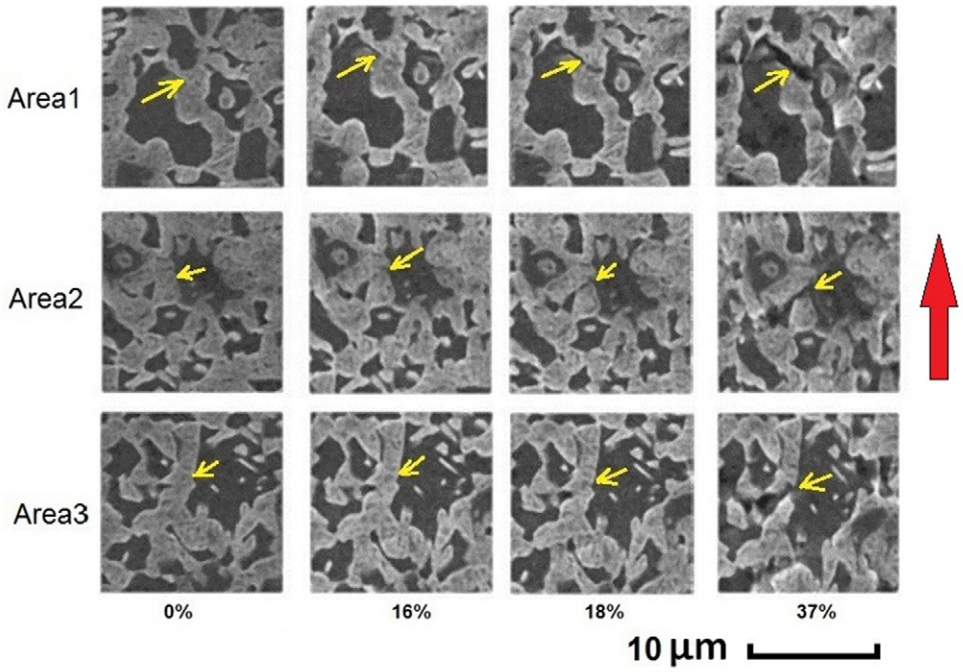

Figure 7. Development of damage in the martensite of DP1000 with the increase of applied specimen strain (%) (the loading direction is shown with the red arrow on the right hand side).

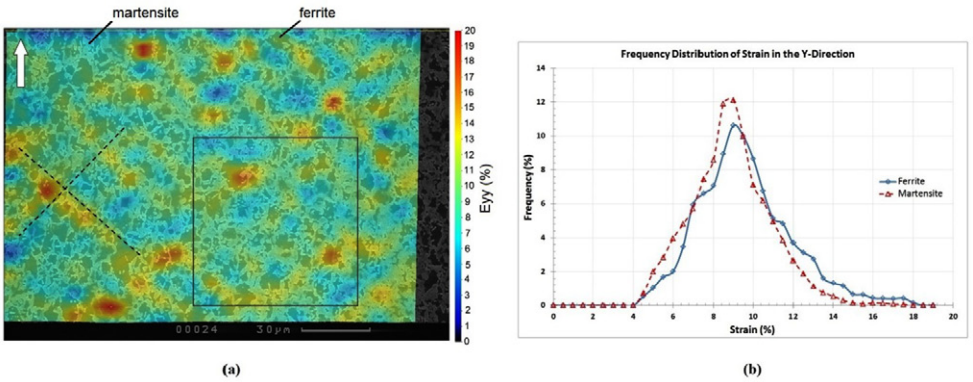

Figure 8. (a) E_{yy} strain (%) map (y-axis along the tensile direction shown by the white arrow) and (b) distribution, over the analysed area of DP1000 at an applied specimen strain of 16%. The two dashed lines in (a) show the strain bands at 45° with respect to the loading direction.

for the simulations (figure 10). Again, the chosen state of deformation corresponded to an applied specimen strain of 16%, as no damage was observed in the microstructure at that stage.

The aim of the simulations was to study the local strain and stress state that initiates fracturing of the martensite through initiation at the interface as was observed experimentally.

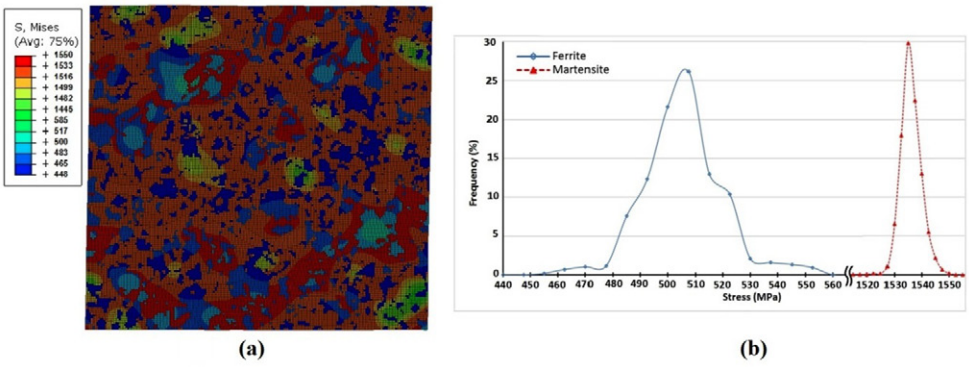

Figure 9. (a) Von Mises stress results and (b) distribution, for microstructure modelling of DP1000 at an applied strain of 16% in the highlighted area of figure 8(a).

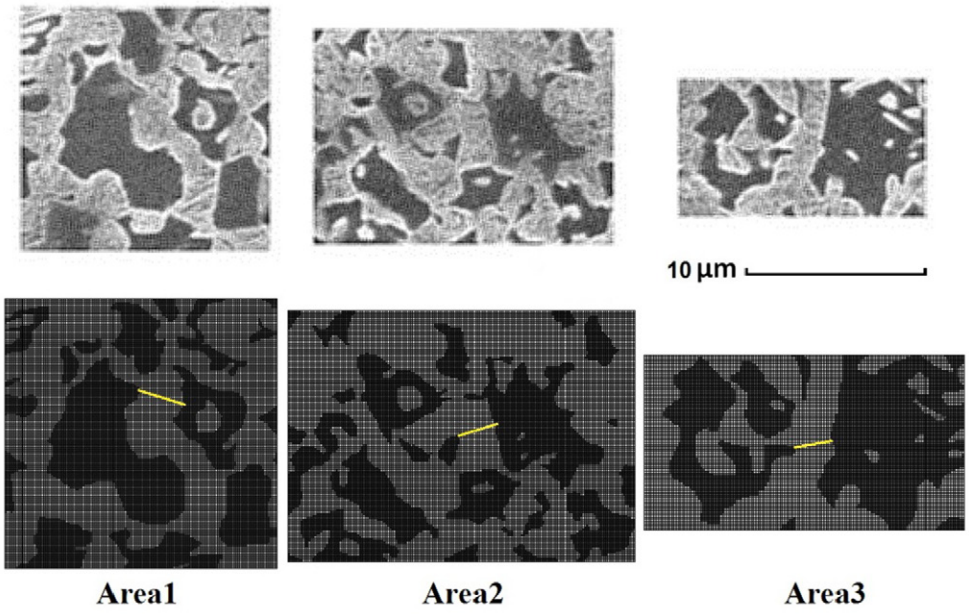

Figure 10. Three FE models (bottom) generated from SEM images (top) to study the stress state of martensite islands before the onset of cracking at the locations highlighted with yellow lines.

Strain and stress levels shown in figure 11 have been set to show the strain along the loading direction E_{yy} and the maximum principal stress distributions in the martensite only. At the location of martensite cracking highlighted in figure 10 with yellow lines, the E_{yy} strain maps in figure 11(a) show values ranging from 14 % in area 2 to 8.6 % in area 3, with therefore no particular correlation between damage events and local strain values. However, as can be seen from figure 11(c) for area 1 and area 3, the highest value of the maximum principal stress was located where a crack appeared during the test (see figure 10). As for area 2, there seems to be more than one location where a potential crack could have appeared according to the FE results. Although a crack did appear at one of these locations (see figure 10), a 3D effect not

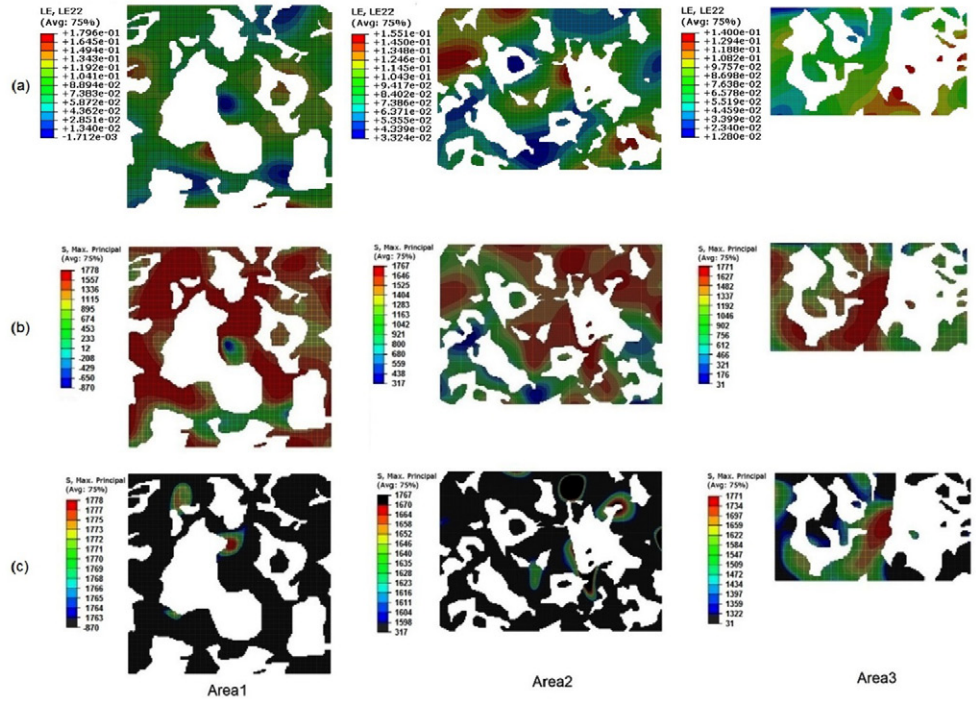

Figure 11. (a) E_{22} strain results (2-axis along the tensile direction, vertical in the images) and (b) maximum principal stress results from the microstructure simulations of the three areas of interest; Stress levels have been selected in (c) to highlight maximum values and the correspondence with crack locations.

taken into account in the simulation might have been responsible for the location selection of crack initiation. The values of maximum principal stress located in the martensite close to the interface with ferrite were all remarkably similar, being 1771 MPa, 1670 MPa and 1722 MPa for area 1, 2 and 3 respectively.

5. Discussion

Results from this work have shown that damage mechanisms in dual-phase steels are influenced by martensite particles and to a lesser degree by inclusions. Avramovic-Cingara *et al* [19] reported that a small number of voids was nucleated as a result of inclusion breaking or decohesion with the matrix in DP600 steels at all strain levels. In that case the voids size was relatively large and only contributed to the increase of void density of the DP-steel rather than being the main failure mechanism. Figure 4 shows an early damage process due to the presence of an inclusion at a small strain value of 2% with eventually the formation of a large void at 16% applied specimen strain. However, in the case observed in this study, the inclusion initiated void did not instigate fracture and played no significant role in the failure of the specimen.

Damage initiated at the interface between the two phases, followed by martensite fracturing was only observed at an applied specimen strain of 16%, as shown in figure 7. This is in agreement with the work by Poruks *et al* [20] who investigated the interface strength and

nucleation strain for void formation due to different particles in steels. Their results show that the strength and thus, nucleation strain, increased in the order of non-metallic particles, Fe_3C carbides and then martensite. This is in agreement with the results reported in this work with voids nucleating around inclusions at low strain, while damage related to martensite islands being observed at higher strain values. The size of the voids created by inclusions was larger than that related to the fracture of martensite islands shown in figure 7, with the latter being more commonly observed during the test. These observations seem to be consistent with findings reported in Avramovic-Cingara [19], even though the specimen strain values cannot be compared directly because of the different sample gauge dimensions used here.

Damage due to martensite regions fracturing has also been reported by Steinbrunner *et al* [21], who claimed that it was the dominant void formation mechanism at strain of 5% in the DP-steel materials they studied. This mechanism was also reported by Kadkhodapoure *et al* [7]. They proposed decohesion of the ferrite/martensite interface as a void initiation mechanism in their model. Avramovic-Cingara *et al* [19] suggested that decohesion between martensite and ferrite was the dominant mechanism of voids nucleation at all strain levels. A possible explanation for these discrepancies is that failure mechanisms are influenced by different factors such as martensite volume fraction, microstructure morphology, chemical composition and manufacturing conditions.

The strain map result in figure 8 is consistent with Ghadbeigi *et al* [6] who reported bands of local strain orientated at around 45° with respect to the loading direction. Furthermore, the similarity of the bell shape distributions of local strain values for both ferrite and martensite shown in figure 8(b), with a slightly higher mean value in the ferrite than in the martensite, is in agreement with the findings of Ghadbeigi *et al* [6] and Han *et al* [22]. This similarity has been explained by Kang *et al* [4] who found that when the size ratio of ferrite islands to the surrounding martensite islands is less than three, the deformation becomes similar for the two phases, as was the case for the DP1000 steel investigated here.

Unlike strain distributions, the von Mises stress distributions in figure 9(b) showed more significant difference between martensite and ferrite, not only in terms of magnitude as expected, but also in terms of standard deviation. Martensite carries stresses up to 1550 MPa, which is consistent with stress results reported by Ramazani *et al* [3, 23]. These authors reported von Mises stress values up to 1700 MPa. However, a direct comparison is not possible because of the difference in carbon contents and morphology between the investigated materials.

In this work, a nucleation criterion for martensite fracturing has been the focus of the microstructural model. Damage in the ferrite was not observed in the analysed area of this investigation, even though this mechanism has been seen on the surface of a specimen towards the end of a tensile test (Ghadbeigi *et al* [6]). This is due to the fact that the centre of the specimen experiences higher stress triaxiality than the surface, which results in a smaller number of voids forming at the surface. Void volume fractions measured using x-ray tomography in DP-steel after necking by Maire *et al* [24] and Landron *et al* [25] indeed showed that the fraction of porosity reached almost zero near the surface, while the maximum void concentration was recorded at the centre of the specimen.

From the DIC and FE results, all strain values such as maximum principal strain, shear strain and strain along the tensile direction, show no correlation between damage locations and local strain values, as can be seen in figure 11(a). This could not be compared to published results as similar studies could not be found in the literature. All stress components have been analysed in the same manner. From the results of maximum principal stress distributions shown in figure 11(c), it is speculated that there may be a correlation between damage location and the value of maximum principal stress at the interface where damage starts. It is therefore

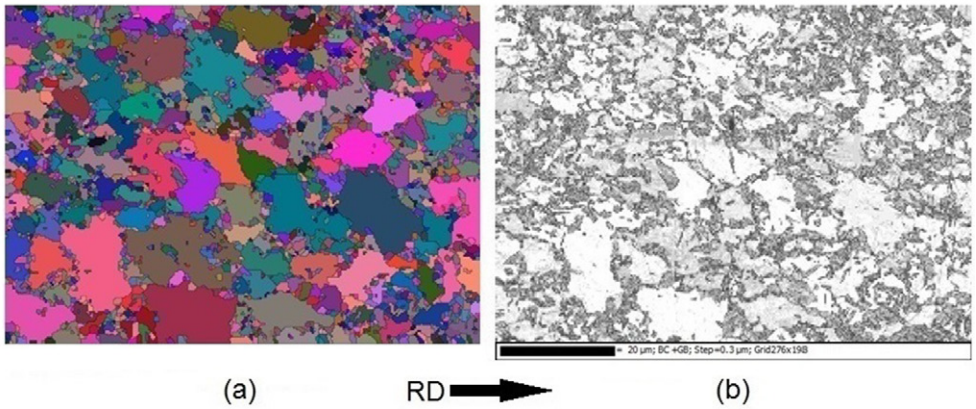

Figure 12. (a) EBSD map of a 75 μm $\times$ 85 μm for DP1000 steel and (b) Band slope map identifying ferrite and martensite.

suggested that a critical maximum principal stress value of about 1700 MPa in the martensite is sufficient to initiate a crack in the martensite.

This finding has important implications for the development of physically-based models of damage development in DP-steels, as this initiation criterion can be used to initiate damage sites in crack propagation models for the prediction of fracture of advanced high strength steels. However, the actual nucleation stress value is likely to be highly dependent on several factors such as the chemical composition of the microstructure constituents at the scale of the microstructure, the volume fraction and spatial distribution of phases as well as crystallographic orientation of grains.

The anisotropy of the material in terms of crystallographic orientations has been characterised using electron-back-scattered-diffraction (EBSD) in a FEG-SEM Zeiss Sigma Microscope. The sample was mechanically grinded and polished down to 0.05 μm (with Colloida Silica). The step size was 0.3 μm, covering approximately a total area of 75 μm $\times$ 85 μm. Figure 12(a) shows the EBSD map of the analysed area, while figure 12(b) shows the band slope map that was used to differentiate martensite from ferrite.

Instead of using the Image Quality map [26, 27], the band slope map was employed here as it differentiates more effectively ferrite from near cubic, but heavily deformed, martensite [28]. The Kikuchi bands during EBSD acquisition are sharper and clearer for the ferrite phase compared to those for martensite. This is because the martensite phase contains a high density of dislocations from the shear mechanism of the phase transformation and to a lesser extent from the tetragonal distortion of the body-centred cubic lattice due to the high concentration of interstitial carbon [26]. A surface area fraction of 60% martensite and 40% ferrite was estimated on the basis of partitioning using the band slope map for the analysed area. A detailed analysis of the orientations within the two phases of the DP steel is shown in figure 13. Figures 13(a) and (b) show the inverse pole figure (IPF) maps for ferrite and martensite respectively. The $\varphi_2 = 45°$ sections of the orientation distribution function (ODF) for ferrite and martensite are shown in figures 13(c) and (d) respectively. The microtexture of both ferrite and martensite is similar in terms of texture components located along the alpha-fiber (RD//$\langle 1\,1\,0\rangle$) and gamma-fiber (ND//$\langle 1\,1\,1\rangle$) but the intensity is generally weaker in the martensite phase (maximum ODF value of 4.5 times random as opposed to 9.8 times random in the ferrite phase).

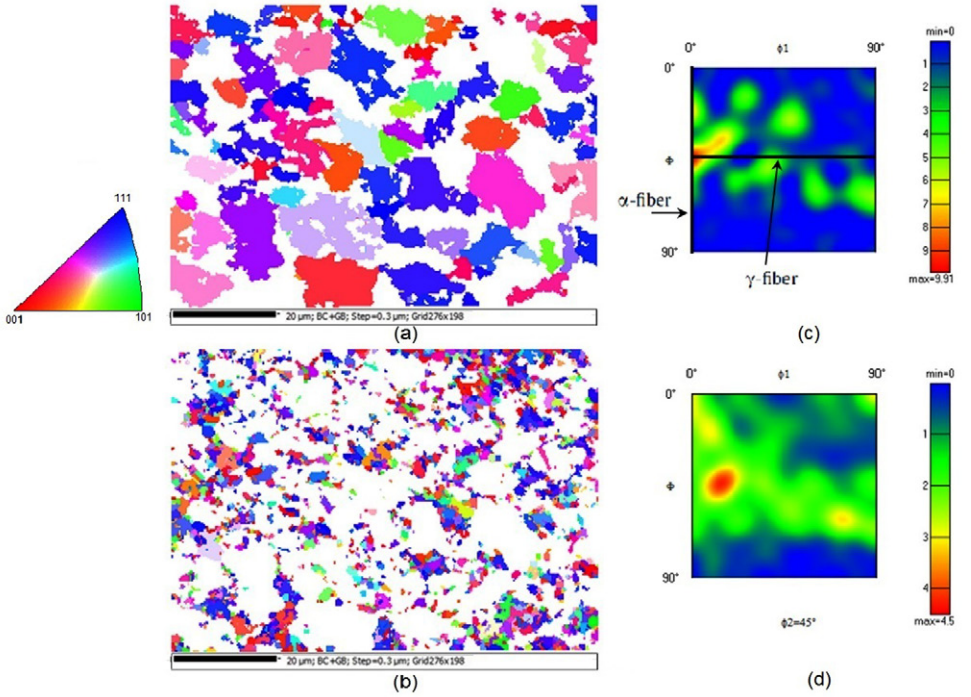

Figure 13. Texture measurements of undeformed DP1000 steel with (a) Inverse pole figure map for ferrite, (b) for martensite, and (c) $\varphi_2 = 45°$ section of the ODF for ferrite and(d) for martensite.

These results show a marked texture in both phases of the DP steel investigated in this work, which are in line with EBSD measurements reported by Choi *et al* [26] (maximum ODF values of 8.4 and 8.2 times random in ferrite and martensite respectively), even though the texture in the martensite phase is weaker in the present study. Stress distributions computed from both a crystal plasticity FEM (CPFEM) and an isotropic elasto-plastic model used to simulate the deformation of the microstructure of a DP980/1000 during a tensile test were compared in Choi *et al* [26]. Results showed an increase of 14% for the maximum stress in martensite after using a CPFE model while an increase of only 8% was recorded for the maximum stress in the ferrite phase. Therefore, stress values computed in the microstructure of the two-phase steel investigated in this work are likely to be inaccurate given the isotropic assumption made in the model.

Apart from the effect of crystallographic orientation, the assumption of 2D plane stress conditions, as assumed in most similar studies found in the literature (e.g. [29, 30]), given the lack of knowledge about the geometry of the microstructure in the third dimension, is another source of uncertainty for the computed stress values. Consequently, stress values calculated in this work should be taken with caution. Despite these uncertainties, a critical value of maximum principal stress distributions matching the location of crack nucleation in martensite seems plausible from the results obtained in this work, but also from a physical basis. Therefore, the proposed damage criterion for martensite is of particular value for the modelling of martensite fracture in DP steels, even though more accurate stress calculations could be considered by taking into account, for instance, the crystallographic orientations of the phases.

A separate criterion for void nucleation in ferrite, likely based on a critical strain [5, 19], could not be developed in this work as damage in that phase was not observed during the test. However the approach developed in this work which closely combines DIC measurements and finite element modelling of the deformation of microstructures offers a real opportunity for the development of new insight into damage formation in DP steels.

6. Conclusion

The present research was designed to study and analyse damage mechanisms in DP1000 steels. The results showed that voids nucleated at inclusions at an early stage of deformation, for an applied specimen strain value as low as 2%. However, a more extensive damage mechanism has been observed in this study for the failure of martensite islands, which initiated beyond the UTS at the interface between ferrite and martensite. A new procedure combining experimental results and finite element simulations of the microstructure with boundary conditions directly imported from the DIC measurements has enabled the study of martensite fracture initiation conditions. The results showed that a maximum principal stress threshold value of about 1700 MPa in the martensite close to the interface with ferrite can initiate the failure of martensite islands at locations observed during the *in situ* tensile testing of the investigated DP1000 steel. Results obtained in this work at the micro-scale in DP1000 therefore provides new insight for the understanding of damage development in Advanced High Strength Steels and for the development of predictive physically-based models of the behaviour of both current and next generation automotive steels.

Acknowledgments

The authors would like to thank EPSRC (grant number EP/F023464/1) for financial support and Tata Steel Europe, in IJmuiden, The Netherlands for providing the material for this study. The authors also thank Dr Peter Korgul for his grateful help and support during this work. The first author thanks Saudi Arabian Cultural Bureau, UK and Taibah University, Madinah for sponsoring his research.

References

[1] Byun T S and Kim I S 1993 Tensile properties and inhomogeneous deformation of ferrite martensite dual-phase steels *J. Mater. Sci.* **28** 2923
[2] Sarwar M and Priestner R 1996 Influence of ferrite-martensite microstructural morphology on tensile properties of dual-phase steel *J. Mater. Sci.* **31** 2091
[3] Ramazani A, Mukherjee K, Prahl U and Bleck W 2012 Modelling the effect of microstructural banding on the flow curve behaviour of dual-phase (DP) steels *Comput. Mater. Sci.* **52** 46
[4] Kang J D, Ososkov Y, Embury J D and Wilkinson D S 2007 Digital image correlation studies for microscopic strain distribution and damage in dual phase steels *Scr. Mater.* **56** 999
[5] Ososkov Y, Wilkinson D S, Jain M and Simpson T 2007 *In situ* measurement of local strain partitioning in a commercial dual-phase steel *Int. J. Mater. Res.* **98** 664
[6] Ghadbeigi H, Pinna C, Celotto S and Yates J R 2010 Local plastic strain evolution in a high strength dual-phase steel *Mater. Sci. Eng. A Struct. Mater.* **527** 5026
[7] Kadkhodapour J, Butz A and Rad S Z 2011 Mechanisms of void formation during tensile testing in a commercial, dual-phase steel *Acta Mater.* **59** 2575
[8] Sun X, Choi K S, Soulami A, Liu W N and Khaleel M A 2009 On key factors influencing ductile fractures of dual phase (DP) steels *Mater. Sci. Eng. A Struct. Mater.* **526** 140
[9] LaVision. Davis Strain master Software 2001

[10] Sutton M A, Orteu J-J and Schreier H W 2009 *Image Correlation for Shape, Motion and Deformation Measurements Basic Concepts, Theory and Applications* (New York: Springer)
[11] Bornert M *et al* 2009 Assessment of digital image correlation measurement errors: methodology and results *Exp. Mech.* **49** 353
[12] Ghadbeigi H, Pinna C and Celotto S 2012 Quantitative strain analysis of the large deformation at the scale of microstructure: comparison between digital image correlation and microgrid techniques *Exp. Mech.* **52** 1483
[13] MATLAB 2010 The MathWorks I
[14] Chalon I 2004 Modelling of the microstructural deformation of duplex stainless steel during plane strain compression *Internal Report* Department of Mechanical Engineering: The University of Sheffield
[15] Simulia. Abaqus 6.10. 2010
[16] Kouznetsova V, Geers M G D and Brekelmans W A M 2002 Multi-scale constitutive modelling of heterogeneous materials with a gradient-enhanced computational homogenization scheme *Int. J. Numer. Methods Eng.* **54** 1235
[17] Nemat-Nasser S and Hori M 1999 *Micromechanics: Overall Properties of Heterogeneous Materials* (Amsterdam: Elsevier)
[18] Asgari S A, Hodgson P D, Yang C and Rolfe B F 2009 Modeling of advanced high strength steels with the realistic microstructure-strength relationships *Comput. Mater. Sci.* **45** 860
[19] Avramovic-Cingara G, Saleh C A R, Jain M K and Wilkinson D S 2009 Void nucleation and growth in dual-phase steel 600 during uniaxial tensile testing *Metall. Mater. Trans.* **40A** 3117
[20] Poruks P, Yakubtsov I and Boyd J D 2006 Martensite-ferrite interface strength in a low-carbon bainitic steel *Scr. Mater.* **54** 41
[21] Steinbrunner D L, Matlock D K and Krauss G 1988 Void formation during tensile testing of dual phase steels *Metall. Trans.* **19** 579
[22] Han Q H, Kang Y L, Hodgson P D and Stanford N 2013 Quantitative measurement of strain partitioning and slip systems in a dual-phase steel *Scr. Mater.* **69** 13
[23] Ramazani A, Schwedt A, Aretz A, Prahl U and Bleck W 2013 Characterization and modelling of failure initiation in DP steel *Comput. Mater. Sci.* **75** 35
[24] Maire E, Bouaziz O, Di Michiel M and Verdu C 2008 Initiation and growth of damage in a dual-phase steel observed by x-ray microtomography *Acta Mater.* **56** 4954
[25] Landron C, Bouaziz O, Maire E and Adrien J 2010 Characterization and modeling of void nucleation by interface decohesion in dual phase steels *Scr. Mater.* **63** 973
[26] Choi S H, Kim E Y, Woo W, Han S H and Kwak J H 2013 The effect of crystallographic orientation on the micromechanical deformation and failure behaviors of DP980 steel during uniaxial tension *Int. J. Plast.* **45** 85
[27] Zaefferer S, Romano P and Friedel F 2008 EBSD as a tool to identify and quantify bainite and ferrite in low-alloyed Al-TRIP steels *J. Microsc.* **230** 499
[28] Zhou W and Wang Z L 2007 *Scanning Microscopy for Nanotechnology: Techniques and Applications* (New York: Springer)
[29] Sun X, Choi K S, Liu W N and Khaleel M A 2009 Predicting failure modes and ductility of dual phase steels using plastic strain localization *Int. J. Plast.* **25** 1888
[30] Tasan C C, Diehl M, Yan D, Zambaldi C, Shanthraj P, Roters F and Raabe D 2014 Integrated experimental-simulation analysis of stress and strain partitioning in multiphase alloys *Acta Mater.* **81** 386